

See discussions, stats, and author profiles for this publication at: <https://www.researchgate.net/publication/279777859>

Block Copolymer Response to Photothermal Stress Fields

ARTICLE *in* MACROMOLECULES · JULY 2015

Impact Factor: 5.8 · DOI: 10.1021/acs.macromol.5b00955

READS

30

2 AUTHORS, INCLUDING:



Paweł W Majewski

Brookhaven National Laboratory

41 PUBLICATIONS 307 CITATIONS

[SEE PROFILE](#)

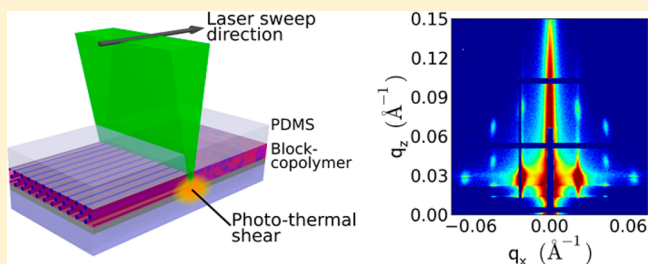
Block Copolymer Response to Photothermal Stress Fields

Pawel W. Majewski* and Kevin G. Yager*

Center for Functional Nanomaterials, Brookhaven National Laboratory, Upton, New York 11973, United States

Supporting Information

ABSTRACT: Block copolymer materials can be aligned using shear forces; in order to fully exploit this phenomenon for controlling nanoscale order, the coupling between applied forces and molecular properties must be elucidated. We use a photothermal method to generate extreme and controllable thermal and stress fields in thin films of cylinder-forming block copolymers. By studying morphological ordering as a function of time, shear rate, polymer material, molecular weight, and film thickness, we elucidate the critical parameters with respect to efficient ordering. We find that ordering efficiency depends weakly on the block copolymer interaction parameter and strongly on the difference in mechanical response of the two phases. Morphologies can be aligned only when the inverse shear rate is smaller than the material's relaxation time. Overall, photothermal shear alignment provides an efficient means of ordering and aligning nanoscale morphologies over macroscopic areas, using a surprisingly short (subsecond) shear pulse.



INTRODUCTION

Block copolymers (BCP) are a well-studied example of self-assembly. Chemical incompatibility between the various regions of the polymer backbone induces phase separation. Yet the covalent connectivity of the polymer architecture frustrates this tendency. The compromise is to form well-defined nanoscale morphology. This powerful paradigm has already demonstrated its potential for the formation of bulk materials,^{1,2} ordered thin films,^{3–5} and functional templates.^{6–9} Although self-assembly easily generates a given nanoscale pattern throughout the sample, the material is typical polygrain, with numerous defects and grain boundaries. Conversely, many applications benefit from large-area uniformity; i.e., it is desirable to generate large grains or even macroscopic alignment of the BCP morphology. A variety of strategies have been presented to improve order in BCP materials. Ordering kinetics can be enhanced using solvent annealing,^{10–13} microwave annealing,^{14–16} or zone annealing.^{17–19} The nanoscale morphology can be aligned using electric,^{20–23} magnetic,^{24–29} or shear^{8,30–37} fields. The morphology can also be controlled using directed self-assembly;^{38,39} that is using corrugated substrates,^{40–42} topographic patterns,^{43–48} or chemical templates.^{49,50} In order to fully exploit these methods, however, one requires fundamental understanding of how the ordering forces couple to polymer properties.

We have recently developed laser zone annealing (LZA),^{19,51} a photothermal method that sweeps a narrow laser line across a polymer thin film. Local photoheating generates large temperatures and extreme in-plane thermal gradients (>3000 °C/mm), which accelerate BCP ordering kinetics by many orders of magnitude. By adding a soft elastic cladding to the polymer film (e.g., polydimethylsiloxane, PDMS), the narrow thermal zone applies a shear field to the BCP film, owing to the

differential thermal expansion of the soft cladding relative to the rigid substrate (e.g., glass). This soft-shear LZA (SS-LZA)⁵² modality thus simultaneously anneals and shears the polymer film (Figure 1a). The extreme photothermal gradients allow access to extreme shear forces; the combination with LZA's enhanced ordering allows simultaneous access to short time scales. Thus, SS-LZA represents a powerful platform for studying how self-assembling materials respond to extreme thermal and mechanical conditions. Herein, we exploit photothermal annealing to elucidate the behavior of block copolymers under extreme conditions. Moreover, we systematically study these trends in order to understand the limitations to achieving high degrees of order in BCP thin films. We find the difference in mechanical properties between the blocks plays a role in ultimate ordering. Importantly, the shear rates must be sufficiently fast so as to overcome the inherent polymer relaxation time scales. Thin film confinement and large molecular weights both hinder alignment, yet the extreme shear rates and thermal fields of SS-LZA are sufficient to order even in these challenging regimes.

RESULTS AND DISCUSSION

The SS-LZA experimental setup is depicted in Figure 1, where a focused laser line is swept across a BCP thin film, thereby photoshearing the material and aligning the nanoscale morphology over macroscopic areas. A typical grazing-incidence small-angle X-ray scattering (GISAXS) image obtained with the X-ray beam aligned along the laser sweep direction is also shown (Figure 1b). The numerous, bright,

Received: May 5, 2015

Revised: June 16, 2015

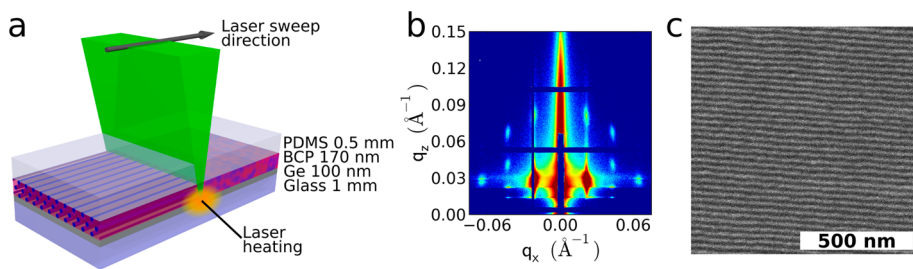


Figure 1. Soft-shear laser zone annealing (SS-LZA). (a) SS-LZA consists of sweeping a focused laser line through a thin film supported on a Ge light-absorbing layer. The local heating anneals the thin film and simultaneously induces differential thermal expansion of a PDMS capping layer. The resultant shear field aligns the as-cast morphology along the laser sweep direction. (b) Example of a GISAXS pattern for a SS-LZA aligned BCP film, measured along the shear direction (cylinder-phase PS-*b*-PMMA, SS-LZA 1× 320 μm/s). (c) Typical SEM image for a SS-LZA aligned film, with the laser sweep horizontal (cylinder-phase PS-*b*-P2VP, SS-LZA 32× 320 μm/s).

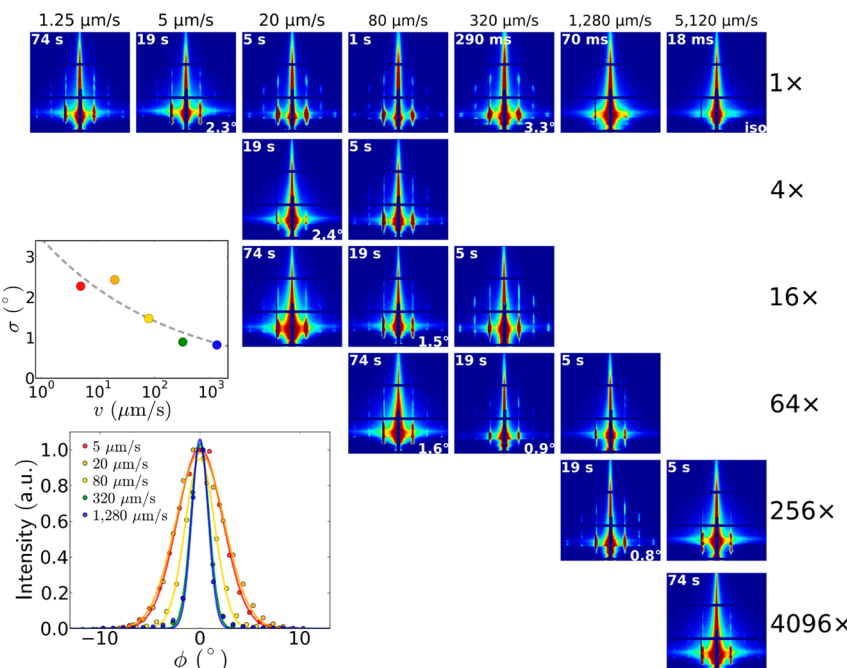


Figure 2. Film processing using SS-LZA. GISAXS images of PS-*b*-PMMA films (170 nm thick) annealed via SS-LZA using a variety of sweep velocities (columns) and number of sweeps (rows). The q -axes are omitted for clarity; they are identical in all cases and consistent with Figure 1 (q_x −0.075 to +0.075 \AA^{-1} ; q_z 0.00 to 0.15 \AA^{-1}). GISAXS images were acquired with the X-ray beam along the sweep direction (where available, the σ orientational spread is given in the lower-right corner); the shearing aligns the cylinders along this axis. The diagonals (upper left to lower right) conserve total annealing time (with the exception of the final row). For a given annealing time (noted in upper-right corner), faster sweeps yield better order. The lower inset shows the GISAXS intensity vs ϕ for total annealing time of 9 s. The upper inset shows the corresponding decrease in σ as shear rate is increased.

higher-order diffraction spots result from the excellent long-range positional order of the nanoscale morphology. We confirm that the morphology is well-aligned with the shear direction by measuring GISAXS as a function of in-plane rotation angle, ϕ . This level of order is especially impressive considering the very short processing time (0.3 s). The quality of alignment can also be assessed using scanning electron microscopy (SEM) to characterize the top surface (Figure 1c). Processing with SS-LZA allows tuning the shear rate using the laser sweep velocity. We estimate the shear rate to be $\dot{\gamma} > 40 \text{ s}^{-1}$ for sweep velocities of $v = 320 \mu\text{m/s}$ (Supporting Information). Figure 2 studies this photoshearing phenomenon in detail, exploring both the sweep velocity (columns) and number of repeated sweeps (rows) of the laser line (diagonals from upper left to lower right thus conserve total processing time). Not surprisingly, longer total shearing times lead to progressively improved order. Very short processing (<100 ms annealing)

yields only very weak order. The quality of sample ordering can be assessed by examining the GISAXS patterns, where bright and sharp peaks are indicative of well-defined nanoscale morphology, while peak sharpness implies long-range coherence of positional order. This can be quantified using a Scherrer analysis to convert from peak width to correlation length (“grain size”)⁵³ and by measuring the width of the orientational spread in the ϕ -direction by rotating the sample (σ denotes the standard deviation of this angular spread). With respect to total annealing time, it is clear that shear ordering saturates after sufficient processing time; remarkably, for SS-LZA, uniaxial alignment throughout the entire sample can be achieved in ~0.3 s, while a saturation of correlation length is observed within ~20 s. In this sense, total annealing time has a relatively weak effect as long as the processing time is long enough for uniaxial alignment to be induced. However, it is also clear that changing sweep speed and number of sweeps is not equivalent:

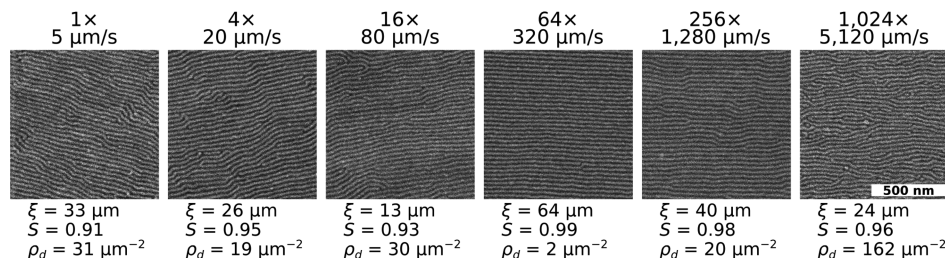


Figure 3. SEM images of SS-LZA processed PS-*b*-P2VP. Thin films (170 nm) were processed using SS-LZA at various sweep velocities (noted above images), with the number of repeated sweeps adjusted to maintain a total annealing time of 9 s. Laser sweep was horizontal across images. Quantitative measures of film quality are noted below images: in-plane orientational correlation length (ξ) and order parameter (S) and the areal density of defects (ρ_d). Increasing shear rate improves the alignment of the morphology (consistent with GISAXS). The order decreases in quality above 320 $\mu\text{m}/\text{s}$ because the sweep velocity counteracts local heat accumulation, reducing the overall annealing temperature (500 nm scale bar applies to all images).

for a given total processing time, faster sweep velocities yield improved order (Figure 3). This trend breaks down at large velocities since rapid motion of the sample counteracts local heat buildup; i.e., reducing the effective processing temperature of course slows the ordering process. Within the regime where temperature is consistent ($v < 1280 \mu\text{m}/\text{s}$),¹⁹ we nevertheless observe a velocity dependence. The insets to Figure 2 show that the orientational spread of the cylinder morphology (relative to the sweep direction) becomes sharper as velocity is increased. Thus, shear alignment is strongly sensitive to the shear rate. We also note that for the highest sweep velocities investigated here ($v = 5120 \mu\text{m}/\text{s}$, $\dot{\gamma} > 700 \text{ s}^{-1}$), a sufficient number of repeated sweeps can in fact lead to aligned, ordered morphologies (Figures 2 and 3). This demonstrates that the polymer film can respond to mechanical stresses even within very short processing events (18 ms).

This result can be contrasted to previous studies of shear alignment of BCP films. Singh et al.⁵² and Qiang et al.^{34,35} both observed decreased quality of alignment at large shear rates, which was attributed to an insufficient time scale for the material to respond to the ordering forces. Our photoshear results suggest that this can be overcome with sufficiently large shear rates and local temperatures. That is, in some regimes the block copolymer can respond to stress fields on millisecond time scales. In fact, as we shall show below, if the shearing time scale is too long, the material becomes unresponsive to shearing.

In order to understand in detail how shear rate couples to BCP response, we used SS-LZA to shear align a variety of BCP materials (Figure 4). The series includes cylinder-forming BCPs of roughly similar molecular weight, with the majority phase being polystyrene (PS) in all cases, but with different minority phases. As can be seen, different BCP materials respond differently to photoshearing. Some materials are easier to shear align than others. Interestingly, some materials appear more “responsive” in the sense that the ordering is strongly sensitive to sweep velocity (e.g., PS-*b*-PI), while other materials are relatively insensitive to velocity (e.g., PS-*b*-PMMA).

The pronounced difference in ordering is quantified in Figure 5b, where the GISAXS-derived in-plane positional correlation length (ξ) is plotted as a function of sweep velocity. Evidently, PS-*b*-PMMA is relatively insensitive to shear rate, while PS-*b*-PI is strongly sensitive and achieves better order than PS-*b*-PMMA for large sweep velocities. We note that the correlation length derived from X-ray scattering is a rather stringent test of film order. For instance, PS-*b*-PI at low sweep velocities (5 $\mu\text{m}/\text{s}$) is poorly ordered (small ξ) but nevertheless is well phase-

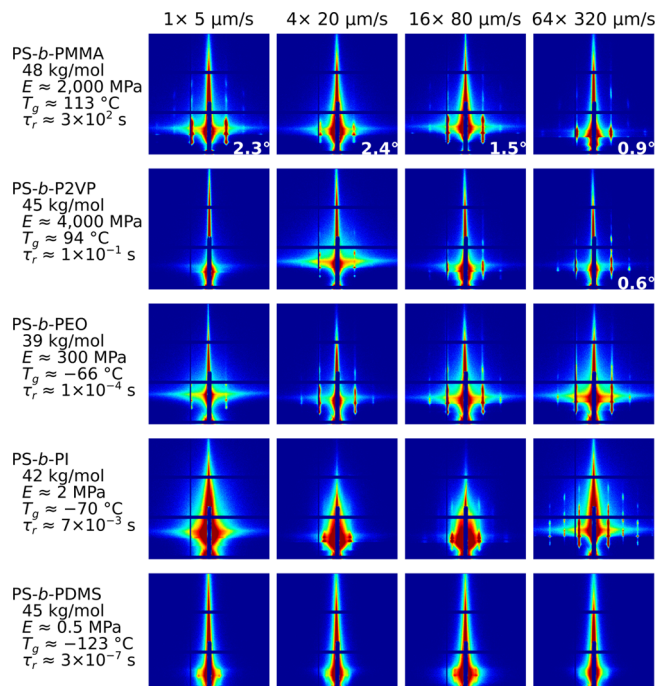


Figure 4. Materials dependence of SS-LZA. GISAXS patterns (along sweep direction) for various BCPs annealed for a total of 9 s (q -axes consistent with Figure 1). Each row corresponds to a different BCP, as noted. Also indicated is the approximate modulus (E) and glass-transition temperature (T_g) of the minority block and the estimated relaxation time of the BCP (τ_r) at ~200 °C. Clearly, the different BCPs respond differently to shear. Whereas PS-*b*-PMMA is relatively shear-insensitive, BCPs with softer minority phases exhibit a strong dependence on sweep velocity.

separated and preferentially aligned (SEM in Figure 5c) over macroscopic areas. The correlation length measured by scattering probes the long-range positional registry of the morphology, whereas SEM imagery instead highlights the persistence of orientational correlations over relatively large areas. PS-*b*-PDMS appears not to become well-ordered under any of the velocities studied.

Block copolymer morphologies respond to shear due to the difference in mechanical properties of the two blocks as well as the block chemical incompatibility.^{8,32} The latter effect, usually defined in terms of the interaction parameter χ , can define the alignment direction: the morphology aligns to minimize the increase in interfacial area during shear flow. For cylinders, this aligns the long axis with the laser-sweep direction, since in this

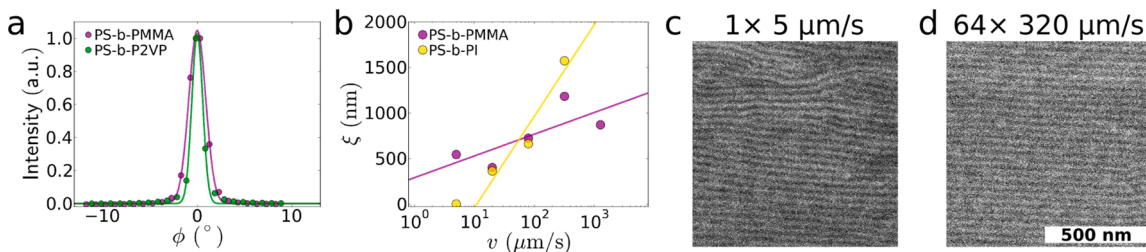


Figure 5. Ordering quality for different BCP materials. All results are for total annealing time of 9 s. (a) Under identical processing conditions, PS-*b*-P2VP becomes slightly more strongly aligned than PS-*b*-PMMA. (b) Positional correlation lengths (ξ) as a function of velocity for two BCP materials (solid lines are log fits, meant as guides to the eye). PS-*b*-PI, which has a much softer minority block, is more strongly ordered (larger correlation length), at high sweep velocities. This softer material is correspondingly more responsive to velocity. (c) SEM of PS-*b*-PI ordered at low sweep speed, displaying relatively poor orientational order. (d) SEM of PS-*b*-PI ordering using high shear rates, where strong alignment is evident.

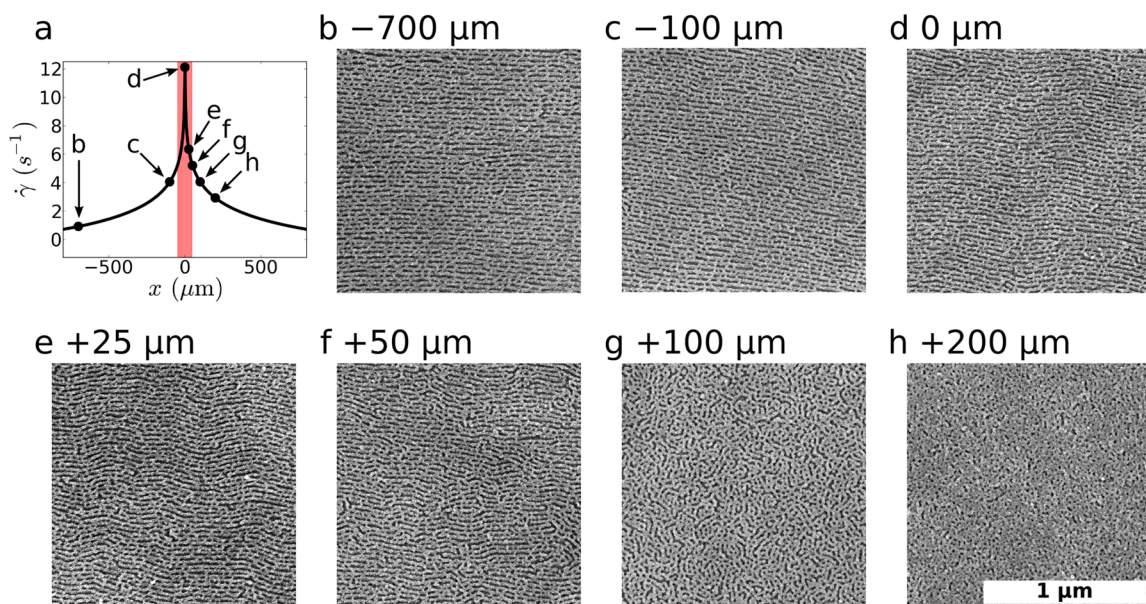


Figure 6. Evolution of order during a SS-LZA experiment (80 $\mu\text{m}/\text{s}$ sweep across 170 nm film of PS-*b*-PMMA). The laser illumination was abruptly terminated during an SS-LZA experiment, which essentially “freezes in” the history of ordering as a function of position. (a) An estimate of the shear rate as a function of position through the sample (and thus as a function of time through an SS-LZA experiment) is plotted (refer to Supporting Information for details). The red band denotes the fwhm of the driving thermal profile; the positions of the SEM images are noted ($x = 0$ is the center of the laser line at termination). (b–h) SEM images through the history of an SS-LZA ordering sweep.

configuration shear-induced flow of BCP chains does not distort the unit cell and thus does not change the interfacial area. On the other hand, the magnitude of the material response may not be dominated by χ . Indeed, the trend we observe does not match the trend in χ for these materials (refer to Supporting Information), nor does it match the trend of order-disorder transition temperatures (T_{ODT}). Some of the materials studied may, in fact, be temporarily driven into the disordered part of the phase diagram during the SS-LZA processing (e.g., PS-*b*-PI). However, even these materials can be efficiently aligned because the strong shear forces of SS-LZA are present on both the advancing and receding fronts. Thus, even materials with low T_{ODT} will experience strong shear alignment from the moment they begin to phase separate (at T_{ODT}) until the moment where polymer mobility is arrested (at T_g). The results do not suggest that T_{ODT} plays an important role: e.g., both PS-*b*-PI and PS-*b*-P2VP exhibit qualitatively similar response to sweep velocity, despite having very different T_{ODT} . A variety of other material properties for the studied BCPs and homopolymer components are summarized in the Supporting Information. Figure 4 lists some parameters that

match the observed ordering trends: the glass-transition temperature (T_g) of the minority blocks, the room-temperature elastic modulus (E) of the minority block, and the estimated relaxation time of the morphology (τ_r) for the studied BCPs at ~ 200 °C (refer to Supporting Information for estimation methods and references). The morphological relaxation time is estimated based on the time scale for a BCP chain to diffuse over a distance scale of roughly the BCP repeat spacing³⁷ (see Supporting Information Figure S10 for temperature-dependent estimate). Of course, it is not surprising that these different material properties all match the experimental trend, since they are interrelated. All of them essentially probe the dynamical response (stiffness vs softness) of the materials.

Shearing can also be rationalized in terms of mechanical and energetic response: the material is orienting in order to minimize energy dissipation during shear. It has been previously reported that the contrast in modulus between the majority and minority phase of a BCP can affect shear alignment response.^{54–56} In materials with a large mechanical contrast, there is a strong preference for alignment of the BCP morphology in a parallel orientation, since this allows for the

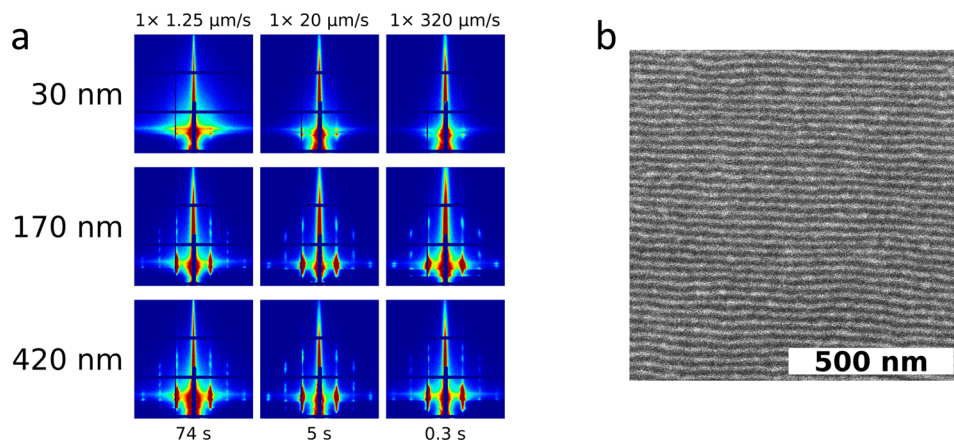


Figure 7. Thickness dependence of SS-LZA. (a) GISAXS of SS-LZA applied across a range of film thicknesses (q -axes consistent with Figure 1) for PS-*b*-PMMA. Each column represents to a different laser sweep velocity (noted above), corresponding to a different processing time (noted below). Although ultrathin (30 nm, monolayer) films are difficult to order, they can nevertheless be aligned. Thicker films respond strongly to shear fields. (b) SEM image of a monolayer of PS-*b*-P2VP cylinders, aligned using SS-LZA (32× 320 μm/s); sweep direction is horizontal across image.

applied strain to be preferentially distributed in the softer component. Thus, materials with larger mechanical contrast will respond more strongly to shear stresses. The relaxation time provides a more complete explanation of the observed trends. In general, one can expect that a material with a relaxation time smaller than the shearing time scale (inverse shear rate) will not respond to shear alignment, since the material is able to relax and dissipate the strain field faster than the stresses are generated. This is precisely what we experimentally observe. PS-*b*-PMMA exhibits slow dynamics, with a relaxation time that is always larger than the experimental time scales. As such, it must respond to the shear stresses through reorientation and is insensitive to shear rate (SS-LZA sweep velocity). On the other extreme, PS-*b*-PDMS is an extremely mobile material, with correspondingly small relaxation times. The material is unaffected by the available shear rates, since the material can rapidly dissipate the shear stresses. Conceivably, much larger shear rates ($\dot{\gamma} > 10^6 \text{ s}^{-1}$) could align this material. For some materials (PS-*b*-PVP, PS-*b*-PEO, and PS-*b*-PI), we observe a strong dependence on shear rate. These materials have a relaxation time commensurate with the experimental inverse shear rate. Thus, when the shearing is too slow, the material relaxes instead of aligns. When the shearing is performed faster than the relaxation time scale, the material instead must realign.

We note that χ likely plays a role in the material response. For instance, PS-*b*-PMMA and PS-*b*-P2VP have fairly similar mechanical contrast; the fact the latter achieves better order under shear (Figure 5a) may be due to its larger χ . From an engineering perspective, this suggests how one should optimize for efficient shear control of nanoscale morphologies: emphasize materials with strong contrast in mechanical properties and χ , and exploit large shear rates. In particular, shear rates must be sufficiently large that the BCP material cannot relax on the time scale of the shearing. SS-LZA provides one convenient route to accessing large shear rates and thus potentially ordering relatively soft and mobile materials.

To understand the mechanism of ordering *during* soft-shear laser zone annealing, we investigated samples where the photothermal processing was abruptly terminated by deactivating the laser illumination. As a result, the temporal history of SS-LZA ordering is “frozen” into the sample,¹⁸ as a function of position from the termination point. From this, it is evident that the SS-LZA ordering occurs during the short time when

the shear rate spikes, which necessarily coincides with the maximum temperatures of the photothermal heating. Even just 200 μm in advance of the laser line, the film is completely disordered and indistinguishable from the as-cast state (Figure 6h). This is despite the fact that the tail of the thermal field extends into this region, which should lead to a stress field in the PDMS cladding and the BCP film. Nevertheless, the BCP film in this region is below the glass-transition temperature (T_g) and thus cannot deform in response to the stress field. As the film crosses through T_g , phase separation begins and disordered BCP domains are observed (Figure 6g). Subsequently, the shear rate dramatically increases, and the BCP film becomes shear-aligned. During these initial stages of alignment, there are undulations in the orientation of the BCP domains (Figure 6d–f). This likely arises from the complex time-varying shear and flow fields in the BCP layer; for instance, as the BCP film is being aligned, it is also undergoing thermal expansion, which is constrained both in the vertical direction (by the substrate and PDMS layers) and in-plane (by the sub- T_g polymer outside the hot zone). As the film passes through the center of the laser line (Figure 6d), the enormous shear rate efficiently aligns the morphology, suppressing the undulations and rapidly eliminating topological defects. This yields a highly ordered, uniaxially aligned morphology (Figure 6b,c). Thus, ordering predominantly occurs on the leading edge of the thermal zone, with the trailing (cooling) edge serving only to slightly improve order. All of the ordering occurs within ~100 μm of the laser line, with the shear alignment predominantly occurring near the center of the thermal zone, where the shear rate is maximized.

Rapid photoshear alignment of BCP morphologies is possible across a range of film thicknesses (Figure 7). Interestingly, thicker films appear to order somewhat more readily; conversely, monolayers of in-plane cylinders are more difficult to efficiently order. Naively, shear forces are expected to be stronger in thinner films: for a given amount of displacement of the elastic PDMS cladding (relative to the rigid substrate), a thinner film experiences a larger shear strain. On the other hand, polymer material close to interfaces may be immobilized and difficult to reorient. Strong thin film confinement thus appears to hinder shear alignment. Previous studies⁵² have similarly observed that shear-induced alignment is less effective in ultrathin films; the fact that SS-LZA is nevertheless able to achieve excellent alignment in monolayer

BCP films represents a key advantage of this technique. Figure 7b shows a highly aligned monolayer of BCP cylinders. We emphasize the utility of being able to easily order ultrathin films. Although it is well-known that BCP materials respond efficiently to shear, it is not trivial to apply efficient shear fields to thin films. SS-LZA provides a relatively simple means of applying a tunable shear force.

Larger molecular weight (MW) materials are more difficult to order. For instance, grain growth rates during oven-annealing decrease sharply with increasing MW. This is due to the hindered dynamics since high-MW systems have more chain entanglements as well as the larger amount of material which must reorganize in a concerted fashion in order to eliminate topological defects. However, even relatively large MW materials can be shear-aligned using SS-LZA (Figure 8), even

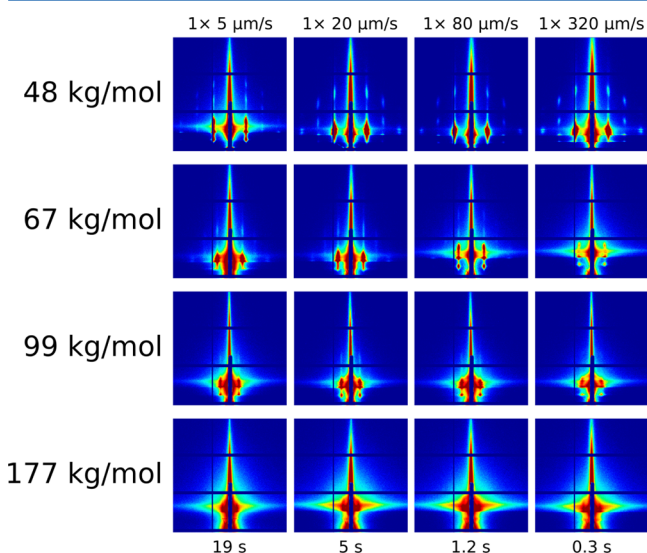


Figure 8. Molecular weight dependence. GISAXS images for PS-*b*-PMMA materials of various molecular weights (*q*-axes consistent with Figure 1). The columns correspond to different sweep velocities (a single laser sweep used in all cases). Higher molecular weights are more difficult to order. Nevertheless, SS-LZA is able to order and align even quite high molecular weight materials.

though these polymer materials are highly entangled. This MW series is consistent with the previous results: larger sweep velocities appear to be more efficient with respect to ordering. In Figure 8, total annealing time is not conserved across the rows. The ultrafast ($v = 320 \mu\text{m/s}$; $\sim 0.3 \text{ s}$ annealing) photoshear is able to achieve order equal to the much slower and longer processing ($v = 5 \mu\text{m/s}$; $\sim 20 \text{ s}$ annealing). Thus, SS-LZA provides a convenient means of rapidly ordering otherwise intractable large-MW materials, where conventional oven annealing is grossly insufficient. This has implications for a wide range of applications that demand large lattice repeats, with nanoscale order aligned over large areas (e.g., for engineered optical response).

CONCLUSION

In summary, we have systematically explored rapid photo-thermal shearing of BCP films. We observe that BCPs exhibit a strong response to shear rate, with improved ordering (larger in-plane positional correlations and narrower orientation distributions) occurring at large laser sweep velocities. Moreover, different BCP materials respond differently. Materials with

larger contrast in mechanical properties (between the majority and minority phases) respond more strongly to shear. Materials also exhibit sensitivity to shear rate, when their inherent relaxation times are commensurate with the experimental time scales. Laser zone annealing coupled to soft-shear effects is able to order and align a wide range of materials, across a range of film thicknesses and molecular weights. Moreover, it is able to produce uniaxially aligned nanoscale morphologies over macroscopic areas, after exceedingly short (subsecond) processing times. Under optimized conditions, defect densities can be extremely low. Thus, SS-LZA is ideally suited to provide robust, versatile, and facile ordering of arbitrary BCP materials.

METHODS

Polymer Films. Substrates were glass slides (1 mm thick, BK-7 FisherFinest) coated with 100 nm of germanium (Ar-plasma sputtered), which acts as a light-absorbing layer. Cylinder-forming block copolymers were obtained from Polymer Source, Inc. A variety of BCP materials are investigated; we use the following abbreviations: polystyrene (PS), poly(methyl methacrylate) (PMMA), poly(2-vinylpyridine) (PVP), poly(ethylene oxide) (PEO), polyisoprene (PI), and polydimethylsiloxane (PDMS). Films were spin-cast from toluene solutions (typical conditions: solutions of ~ 3 wt %, 1000 rpm). Where not otherwise noted, films were 170 nm thick (measured using optical interferometry). Films were dried under vacuum at 60°C for 4 h to remove residual solvent.⁵⁷ Samples were diced into $12 \times 12 \text{ mm}^2$ squares.

Laser Zone Annealing. We have previously reported in detail the laser zone annealing (LZA) setup.¹⁹ Briefly, a green (532 nm) laser (3 W, Melles Griot 85 GHS 309) was focused using a three-lens system into a sharp line at the sample position ($20 \mu\text{m}$ fwhm $\times \sim 20 \text{ mm}$ breadth). The laser light is absorbed by the Ge substrate layer, leading to local heating and thermal gradients. By translating the sample through the laser line, a thermal zone is swept through the film. Because of the nontrivial thermal history experienced by any given film location, we characterize the annealing conditions using the half-height of the thermal spike. The thermal zone has a fwhm of $\sim 90 \mu\text{m}$ and a temperature (at half-maximum) of $T_{\text{HM}} \approx 270^\circ\text{C}$ and induces thermal gradients of $\nabla T_{\text{HM}} \approx 1500^\circ\text{C/mm}$ (with $\nabla T > 3000^\circ\text{C/mm}$ near the peak). The local annealing time depends on the sweep velocity (and the number of repeated sweeps). For the sweep velocities described in this paper, the local annealing time is sufficiently short that no measurable amount of polymer degradation is observed, despite the extreme processing temperatures.

Soft-Shear LZA. For soft-shear (SS) experiments, cross-linked polydimethylsiloxane pads (PDMS, Sylgard 184 with 5:1 mix ratio, vacuum-cured at 80°C for 24 h) of 0.5 mm thickness were placed on top of the polymer films, where it achieves conformal contact with the BCP surface. Samples were then processed using LZA; the soft elastic PDMS cladding undergoes differential thermal expansion (with respect to the rigid glass substrate), generating shear-fields in the polymer thin film. The PDMS capping reduces the LZA temperatures by $\sim 50^\circ\text{C}$, confirmed by both experimental measurement and numerical simulation.⁵⁸ The maximum temperature during an SS-LZA experiment is 430°C , with this temperature maintained only for an infinitesimal time. Refer to the Supporting Information for estimates of the temperature, strain, stress, and shear fields during SS-LZA.

GISAXS. Synchrotron grazing-incidence small-angle X-ray scattering (GISAXS) experiments were performed at the X9 undulator beamline of the National Synchrotron Light Source at Brookhaven National Laboratory. Two-dimensional scattering images were collected using a fiber-taper charge-coupled device (MarCCD) or a hybrid pixel-array detector (Dectris Pilatus 1M). Samples were measured under vacuum using an X-ray beam of 13.5 keV ($\lambda = 0.0918 \text{ nm}$). GISAXS data were collected across a range of incidence angles (0.07° – 0.20°). The data presented in the article are for 0.12° (the structures implied by GISAXS were not dependent on incident angle). Silver behenate powder was used as a standard for data

conversion to q -space. A laser beam reflected from the sample surface was used to level each sample, with respect to the ϕ -rotation stage, to ensure that the samples remained aligned with the X-ray beam during in-plane rotations. This proper alignment was confirmed by ensuring both that the reflected laser beam was invariant upon rotation and that the GISAXS patterns (e.g., position of Yoneda band) were similarly stable upon large rotation ($\pm 90^\circ$). Samples for GISAXS rotation analysis were diced and cleaned to yield a $\sim 4\text{ mm} \times 4\text{ mm}$ patch near the center of the original substrate. This ensures that sample edge effects are eliminated and that the scattering volume remains roughly constant during large ϕ rotations. Average in-plane correlation length ("grain size") was estimated using a Scherrer peak width analysis, after accounting for peak broadening contributions from instrumental and grazing-incidence aspects.⁵³ We emphasize that the appearance of bright peaks in scattering images is a particularly stringent test of the quality of thin-film morphology. The beam projection of the grazing-incidence geometry means that the GISAXS results are a statistical average over a $100\text{ }\mu\text{m} \times 4\text{ mm} = 0.4\text{ mm}^2$ area. Moreover, comparing corresponding GISAXS and SEM data (e.g., Figures 3 and 4), it is clear that even with well-defined local ordering evident in SEM (and giving rise to a first-order GISAXS peak), only exceptionally well-defined long-range positional registry can give rise to higher-order scattering peaks.

SEM. Thin film surface morphology was characterized using a Hitachi S-4800 scanning electron microscope (SEM). To highlight the underlying morphology, samples of in-plane cylinder phases must be processed. For PS-*b*-P2VP and PS-*b*-PI, samples were exposed to iodine vapor for 30 min, which improves the imaging contrast between the majority and minority BCP phases. For PS-*b*-PMMA, samples were UV-irradiated to cross-link the majority (PS) phase, followed by brief O₂ plasma treatment (Nordson CS-1701, 100 mT, 20 W), to remove the PS wetting layer and etch the PMMA domains. Images were analyzed in order to extract a variety of quantitative measures of the quality of morphological ordering and alignment. The in-plane orientational correlation length (ξ) is estimated by evaluating the anisotropy in local image gradients to compute an orientation map and then fitting the average spatial decay of orientation to an exponential function.^{17–19} The histogram of orientations can also be analyzed to compute the Hermans orientational order parameter (S), where $S = 1$ indicates perfect uniaxial alignment and $S = 0$ indicates a random (isotropic) orientation distribution. The reported measurements in the paper average over 5–10 different images. We also estimate the areal density of topological defects (ρ_d), i.e. disclinations or dislocations, by manually tagging these features in representative images and dividing by total image area.

ASSOCIATED CONTENT

Supporting Information

Figures S1–S13. The Supporting Information is available free of charge on the ACS Publications website at DOI: 10.1021/acs.macromol.5b00955.

AUTHOR INFORMATION

Corresponding Authors

*E-mail: pmajewski@bnl.gov (P.W.M.).

*E-mail: kyager@bnl.gov (K.G.Y.).

Notes

The authors declare no competing financial interest.

ACKNOWLEDGMENTS

Research was carried out at the Center for Functional Nanomaterials, and National Synchrotron Light Source, Brookhaven National Laboratory, which are supported by the U.S. Department of Energy, Office of Basic Energy Sciences, under Contract DE-SC0012704.

REFERENCES

- (1) Ruzette, A.-V.; Leibler, L. Block Copolymers in Tomorrow's Plastics. *Nat. Mater.* **2005**, *4*, 19–31.
- (2) Bates, F. S.; Fredrickson, G. H. Block Copolymer Thermodynamics: Theory and Experiment. *Annu. Rev. Phys. Chem.* **1990**, *41*, 525–557.
- (3) Fasolka, M. J.; Mayes, A. M. Block Copolymer Thin Films: Physics and Applications. *Annu. Rev. Mater. Res.* **2001**, *31*, 323–355.
- (4) Stein, G. E.; Mahadevapuram, N.; Mitra, I. Controlling Interfacial Interactions for Directed Self Assembly of Block Copolymers. *J. Polym. Sci., Part B: Polym. Phys.* **2015**, *53*, 96–102.
- (5) Kim, H.-C.; Hinsberg, W. D. Surface Patterns from Block Copolymer Self-Assembly. *J. Vac. Sci. Technol., A* **2008**, *26*, 1369–1382.
- (6) Hamley, I. W. Ordering in Thin Films of Block Copolymers: Fundamentals to Potential Applications. *Prog. Polym. Sci.* **2009**, *34*, 1161–1210.
- (7) Bates, C. M.; Maher, M. J.; Janes, D. W.; Ellison, C. J.; Willson, C. G. Block Copolymer Lithography. *Macromolecules* **2014**, *47*, 2–12.
- (8) Hu, H.; Gopinadhan, M.; Osuji, C. O. Directed Self-Assembly of Block Copolymers: A Tutorial Review of Strategies for Enabling Nanotechnology with Soft Matter. *Soft Matter* **2014**, *10*, 3867–3889.
- (9) Darling, S. B. Directing the Self-Assembly of Block Copolymers. *Prog. Polym. Sci.* **2007**, *32*, 1152–1204.
- (10) Seppala, J. E.; Lewis, R. L.; Epps, T. H. Spatial and Orientation Control of Cylindrical Nanostructures in ABA Triblock Copolymer Thin Films by Raster Solvent Vapor Annealing. *ACS Nano* **2012**, *6*, 9855–9862.
- (11) Kim, S. H.; Misner, M. J.; Russell, T. P. Solvent-Induced Ordering in Thin Film Diblock Copolymer/Homopolymer Mixtures. *Adv. Mater.* **2004**, *16*, 2119–2123.
- (12) Kimura, M.; Misner, M. J.; Xu, T.; Kim, S. H.; Russell, T. P. Long-Range Ordering of Diblock Copolymers Induced by Droplet Pinning. *Langmuir* **2003**, *19*, 9910–9913.
- (13) Sinturel, C.; Vayer, M.; Morris, M.; Hillmyer, M. A. Solvent Vapor Annealing of Block Polymer Thin Films. *Macromolecules* **2013**, *46*, 5399–5415.
- (14) Zhang, X.; Harris, K. D.; Wu, N. L. Y.; Murphy, J. N.; Buriak, J. M. Fast Assembly of Ordered Block Copolymer Nanostructures through Microwave Annealing. *ACS Nano* **2010**, *4*, 7021–7029.
- (15) Jin, C.; Murphy, J. N.; Harris, K. D.; Buriak, J. M. Deconvoluting the Mechanism of Microwave Annealing of Block Copolymer Thin Films. *ACS Nano* **2014**, *8*, 3979–3991.
- (16) Borah, D.; Sentharamaikannan, R.; Rasappa, S.; Kosmala, B.; Holmes, J. D.; Morris, M. A. Swift Nanopattern Formation of PS-*b*-PMMA and PS-*b*-PDMS Block Copolymer Films Using a Microwave Assisted Technique. *ACS Nano* **2013**, *7*, 6583–6596.
- (17) Berry, B. C.; Bosse, A. W.; Douglas, J. F.; Jones, R. L.; Karim, A. Orientational Order in Block Copolymer Films Zone Annealed Below the Order-Disorder Transition Temperature. *Nano Lett.* **2007**, *7*, 2789–2794.
- (18) Yager, K. G.; Fredin, N. J.; Zhang, X.; Berry, B. C.; Karim, A.; Jones, R. L. Evolution of Block-Copolymer Order through a Moving Thermal Zone. *Soft Matter* **2010**, *6*, 92–99.
- (19) Majewski, P. W.; Yager, K. G. Millisecond Ordering of Block Copolymer Films Via Photothermal Gradients. *ACS Nano* **2015**, *9*, 3896–3906.
- (20) Ashok, B.; Muthukumar, M.; Russell, T. P. Confined Thin Film Diblock Copolymer in the Presence of an Electric Field. *J. Chem. Phys.* **2001**, *115*, 1559–1564.
- (21) Pereira, G. G.; Williams, D. R. M. Diblock Copolymer Melts in Electric Fields: The Transition from Parallel to Perpendicular Alignment Using a Capacitor Analogy. *Macromolecules* **1999**, *32*, 8115–8120.
- (22) Tsori, Y.; Andelman, D. Thin Film Diblock Copolymers in Electric Field: Transition from Perpendicular to Parallel Lamellae. *Macromolecules* **2002**, *35*, 5161–5170.

- (23) Liedel, C.; Pester, C. W.; Ruppel, M.; Urban, V. S.; Böker, A. Beyond Orientation: The Impact of Electric Fields on Block Copolymers. *Macromol. Chem. Phys.* **2012**, *213*, 259–269.
- (24) Majewski, P. W.; Gopinadhan, M.; Osuji, C. O. Magnetic Field Alignment of Block Copolymers and Polymer Nanocomposites: Scalable Microstructure Control in Functional Soft Materials. *J. Polym. Sci., Part B: Polym. Phys.* **2012**, *50*, 2–8.
- (25) Gopinadhan, M.; Majewski, P. W.; Osuji, C. O. Facile Alignment of Amorphous Poly(Ethylene Oxide) Microdomains in a Liquid Crystalline Block Copolymer Using Magnetic Fields: Toward Ordered Electrolyte Membranes. *Macromolecules* **2010**, *43*, 3286–3293.
- (26) Majewski, P. W.; Gopinadhan, M.; Jang, W.-S.; Lutkenhaus, J. L.; Osuji, C. O. Anisotropic Ionic Conductivity in Block Copolymer Membranes by Magnetic Field Alignment. *J. Am. Chem. Soc.* **2010**, *132*, 17516–17522.
- (27) Osuji, C.; Ferreira, P. J.; Mao, G.; Ober, C. K.; Vander Sande, J. B.; Thomas, E. L. Alignment of Self-Assembled Hierarchical Microstructure in Liquid Crystalline Diblock Copolymers Using High Magnetic Fields. *Macromolecules* **2004**, *37*, 9903–9908.
- (28) McCulloch, B.; Portale, G.; Bras, W.; Pople, J. A.; Hexemer, A.; Segalman, R. A. Dynamics of Magnetic Alignment in Rod–Coil Block Copolymers. *Macromolecules* **2013**, *46*, 4462–4471.
- (29) Majewski, P. W.; Gopinadhan, M.; Osuji, C. O. Understanding Anisotropic Transport in Self-Assembled Membranes and Maximizing Ionic Conductivity by Microstructure Alignment. *Soft Matter* **2013**, *9*, 7106–7116.
- (30) Riise, B. L.; Fredrickson, G. H.; Larson, R. G.; Pearson, D. S. Rheology and Shear-Induced Alignment of Lamellar Diblock and Triblock Copolymers. *Macromolecules* **1995**, *28*, 7653–7659.
- (31) Koppi, K. A.; Tirrell, M.; Bates, F. S. Shear-Induced Isotropic-to-Lamellar Transition. *Phys. Rev. Lett.* **1993**, *70*, 1449.
- (32) Nikoubashman, A.; Register, R. A.; Panagiotopoulos, A. Z. Simulations of Shear-Induced Morphological Transitions in Block Copolymers. *Soft Matter* **2013**, *9*, 9960–9971.
- (33) Nikoubashman, A.; Davis, R. L.; Michal, B. T.; Chaikin, P. M.; Register, R. A.; Panagiotopoulos, A. Z. Thin Films of Homopolymers and Cylinder-Forming Diblock Copolymers under Shear. *ACS Nano* **2014**, *8*, 8015–8026.
- (34) Qiang, Z.; Zhang, L.; Stein, G. E.; Cavicchi, K. A.; Vogt, B. D. Unidirectional Alignment of Block Copolymer Films Induced by Expansion of a Permeable Elastomer During Solvent Vapor Annealing. *Macromolecules* **2014**, *47*, 1109–1116.
- (35) Qiang, Z.; Zhang, Y.; Groff, J. A.; Cavicchi, K. A.; Vogt, B. D. A Generalized Method for Alignment of Block Copolymer Films: Solvent Vapor Annealing with Soft Shear. *Soft Matter* **2014**, *10*, 6068–6076.
- (36) Angelescu, D. E.; Waller, J. H.; Register, R. A.; Chaikin, P. M. Shear-Induced Alignment in Thin Films of Spherical Nanodomains. *Adv. Mater.* **2005**, *17*, 1878–1881.
- (37) Angelescu, D. E.; Waller, J. H.; Adamson, D. H.; Deshpande, P.; Chou, S. Y.; Register, R. A.; Chaikin, P. M. Macroscopic Orientation of Block Copolymer Cylinders in Single-Layer Films by Shearing. *Adv. Mater.* **2004**, *16*, 1736–1740.
- (38) Koo, K.; Ahn, H.; Kim, S.-W.; Ryu, D. Y.; Russell, T. P. Directed Self-Assembly of Block Copolymers in the Extreme: Guiding Microdomains from the Small to the Large. *Soft Matter* **2013**, *9*, 9059–9071.
- (39) Cheng, J. Y.; Ross, C. A.; Smith, H. I.; Thomas, E. L. Templated Self-Assembly of Block Copolymers: Top-Down Helps Bottom-Up. *Adv. Mater.* **2006**, *18*, 2505–2521.
- (40) Kim, H.-C.; Rettner, C. T.; Sundström, L. Fabrication of 20 nm Half-Pitch Gratings by Corrugation-Directed Self-Assembly. *Nanotechnology* **2008**, *19*, 235301.
- (41) Park, S. M.; Berry, B. C.; Dobisz, E.; Kim, H. C. Observation of Surface Corrugation-Induced Alignment of Lamellar Microdomains in PS-b-PMMA Thin Films. *Soft Matter* **2009**, *5*, 957–961.
- (42) Hong, S. W.; Huh, J.; Gu, X.; Lee, D. H.; Jo, W. H.; Park, S.; Xu, T.; Russell, T. P. Unidirectionally Aligned Line Patterns Driven by Entropic Effects on Faceted Surfaces. *Proc. Natl. Acad. Sci. U. S. A.* **2012**, *109*, 1402.
- (43) Segalman, R. A.; Hexemer, A.; Kramer, E. J. Effects of Lateral Confinement on Order in Spherical Domain Block Copolymer Thin Films. *Macromolecules* **2003**, *36*, 6831–6839.
- (44) Sundrani, D.; Darling, S. B.; Sibener, S. J. Guiding Polymers to Perfection: Macroscopic Alignment of Nanoscale Domains. *Nano Lett.* **2004**, *4*, 273–276.
- (45) Sundrani, D.; Darling, S. B.; Sibener, S. J. Hierarchical Assembly and Compliance of Aligned Nanoscale Polymer Cylinders in Confinement. *Langmuir* **2004**, *20*, 5091–5099.
- (46) Hammond, M. R.; Cochran, E.; Fredrickson, G. H.; Kramer, E. J. Temperature Dependence of Order, Disorder, and Defects in Laterally Confined Diblock Copolymer Cylinder Monolayers. *Macromolecules* **2005**, *38*, 6575–6585.
- (47) Ruiz, R.; Ruiz, N.; Zhang, Y.; Sandstrom, R. L.; Black, C. T. Local Defectivity Control of 2D Self-Assembled Block Copolymer Patterns. *Adv. Mater.* **2007**, *19*, 2157–2162.
- (48) Zhang, X.; De Paoli Lacerda, S. H.; Yager, K. G.; Berry, B. C.; Douglas, J. F.; Jones, R. L.; Karim, A. Target Patterns Induced by Fixed Nanoparticles in Block Copolymer Films. *ACS Nano* **2009**, *3*, 2115–2120.
- (49) Yang, X. M.; Peters, R. D.; Nealey, P. F.; Solak, H. H.; Cerrina, F. Guided Self-Assembly of Symmetric Diblock Copolymer Films on Chemically Nanopatterned Substrates. *Macromolecules* **2000**, *33*, 9575–9582.
- (50) Ouk Kim, S.; Solak, H. H.; Stoykovich, M. P.; Ferrier, N. J.; de Pablo, J. J.; Nealey, P. F. Epitaxial Self-Assembly of Block Copolymers on Lithographically Defined Nanopatterned Substrates. *Nature* **2003**, *424*, 411.
- (51) Majewski, P. W.; Rahman, A.; Black, C. T.; Yager, K. G. Arbitrary Lattice Symmetries via Block Copolymer Nanomeshes. *Nat. Commun.* **2015**, *6*, 7448.
- (52) Singh, G.; Yager, K. G.; Berry, B.; Kim, H.-C.; Karim, A. Dynamic Thermal Field-Induced Gradient Soft-Shear for Highly Oriented Block Copolymer Thin Films. *ACS Nano* **2012**, *6*, 10335–10342.
- (53) Smilgies, D.-M. Scherrer Grain-Size Analysis Adapted to Grazing-Incidence Scattering with Area Detectors. *J. Appl. Crystallogr.* **2009**, *42*, 1030–1034.
- (54) Fredrickson, G. H.; Bates, F. S. Dynamics of Block Copolymers: Theory and Experiment. *Annu. Rev. Mater. Sci.* **1996**, *26*, 501–550.
- (55) Patel, S. S.; Larson, R. G.; Winey, K. I.; Watanabe, H. Shear Orientation and Rheology of a Lamellar Polystyrene-Polyisoprene Block Copolymer. *Macromolecules* **1995**, *28*, 4313–4318.
- (56) Zhang, Y.; Wiesner, U.; Spiess, H. W. Frequency Dependence of Orientation in Dynamically Sheared Diblock Copolymers. *Macromolecules* **1995**, *28*, 778–781.
- (57) Zhang, X.; Yager, K. G.; Kang, S.; Fredin, N. J.; Akgun, B.; Satija, S.; Douglas, J. F.; Karim, A.; Jones, R. L. Solvent Retention in Thin Spin-Coated Polystyrene and Poly(Methyl Methacrylate) Homopolymer Films Studied by Neutron Reflectometry. *Macromolecules* **2010**, *43*, 1117–1123.
- (58) Yager, K. G.; Barrett, C. J. Temperature Modeling of Laser-Irradiated Azo-Polymer Thin Films. *J. Chem. Phys.* **2004**, *120*, 1089–1096.